NAVAL POSTGRADUATE SCHOOL
Monterey, California

THESIS

STATISTICAL ANALYSIS OF BACKGROUND IR EMISSION IN THE 3-5.6 μm AND 8-14 μm REGIONS

by

Şefik BAYAR

December 1989

Thesis Advisor: D. D. Cleary

Approved for public release; distribution is unlimited

Unclassified
SECURITY CLASSIFICATION OF THIS PAGE

REPORT DOCUMENTATION PAGE

Form Approved
OMB No. 0704-0188

1a. REPORT SECURITY CLASSIFICATION: UNCLASSIFIED	1b. RESTRICTIVE MARKINGS
2a. SECURITY CLASSIFICATION AUTHORITY	3. DISTRIBUTION / AVAILABILITY OF REPORT: Approved for public release; distribution is unlimited
2b. DECLASSIFICATION / DOWNGRADING SCHEDULE	
4. PERFORMING ORGANIZATION REPORT NUMBER(S)	5. MONITORING ORGANIZATION REPORT NUMBER(S)
6a. NAME OF PERFORMING ORGANIZATION: Naval Postgraduate School; 6b. OFFICE SYMBOL (If applicable): 3A	7a. NAME OF MONITORING ORGANIZATION: Naval Postgraduate School
6c. ADDRESS (City, State, and ZIP Code): Monterey, California 93943-5100	7b. ADDRESS (City, State, and ZIP Code): Monterey, California 93943-5100
8a. NAME OF FUNDING / SPONSORING ORGANIZATION; 8b. OFFICE SYMBOL (If applicable)	9. PROCUREMENT INSTRUMENT IDENTIFICATION NUMBER
8c. ADDRESS (City, State, and ZIP Code)	10. SOURCE OF FUNDING NUMBERS: PROGRAM ELEMENT NO. / PROJECT NO. / TASK NO. / WORK UNIT ACCESSION NO.

11. TITLE (Include Security Classification)

STATISTICAL ANALYSIS OF BACKGROUND IR EMISSION IN THE 3–5.6 μm AND 8–14 μm REGIONS

12. PERSONAL AUTHOR(S): Şefik BAYAR

13a. TYPE OF REPORT	13b. TIME COVERED	14. DATE OF REPORT (Year, Month, Day)	15. PAGE COUNT
Master's Thesis	FROM _____ TO _____	1989 December	67

16. SUPPLEMENTARY NOTATION: The views expressed in this thesis are those of the author and do not reflect the official policy or position of the Department of Defense or the U.S. Government.

17. COSATI CODES			18. SUBJECT TERMS (Continue on reverse if necessary and identify by block number)
FIELD	GROUP	SUB-GROUP	Apparent Radient Emittance; Infrared Background Noise

19. ABSTRACT (Continue on reverse if necessary and identify by block number)

The amplitude distributions of the sky and sea background noise in the 3–5.6 μm and 8–14 μm spectral regions are analyzed. These background scenes were obtained with an AGEMA 780 Thermovision sensor and recorded with the AGEMA TIC–8000 data acquisition system. The amplitude distributions of 3–5.6 μm clear sky, 3–5.6 μm cloudy sky, and 8–14 μm sea background noise sources obey Gaussian distributions. A Gaussian amplitude distribution does not provide a good fit to the observed 3–5.6 μm sea background data and the 8–14 μm clear sky background. Scene contamination may have caused the 3–5.6 μm sea background to deviate from a Gaussian distribution. In addition, the amplitudes of the 8–14 μm clear sky background fall into the non–linear portion of the dynamic range of the scanner. As a result, no conclusion is made regarding the parent distributions for 3–5.6 μm sea background or the 8–14 μm clear sky background.

20. DISTRIBUTION / AVAILABILITY OF ABSTRACT	21. ABSTRACT SECURITY CLASSIFICATION
☒ UNCLASSIFIED/UNLIMITED ☐ SAME AS RPT ☐ DTIC USERS	Unclassified
22a. NAME OF RESPONSIBLE INDIVIDUAL: D.D. Cleary	22b. TELEPHONE (Include Area Code): (408) 646 2828; 22c. OFFICE SYMBOL: 61 Cl

DD Form 1473, JUN 86 — Previous editions are obsolete — S/N 0102-LF-014-6603

SECURITY CLASSIFICATION OF THIS PAGE: Unclassified

Approved for public release; distribution is unlimited.

Statistical Analysis of Background IR Emission
in the $3-5.6\ \mu m$ and $8-14\ \mu m$ Regions

by

Şefik BAYAR
LTJG, Turkish Navy
B.S., Turkish Naval Academy, 1983

Submitted in partial fulfillment of the
requirements for the degree of

MASTER OF SCIENCE IN SYSTEMS ENGINEERING
(ELECTRONIC WARFARE)
from the

NAVAL POSTGRADUATE SCHOOL
December 1989

ABSTRACT

The amplitude distributions of the sky and sea background noise in the 3–5.6 μm and 8–14 μm spectral regions are analyzed. These background scenes were obtained with an AGEMA 780 Thermovision sensor and recorded with the AGEMA TIC–8000 data acquisition system. The amplitude distributions of 3–5.6 μm clear sky, 3–5.6 μm cloudy sky, and 8–14 μm sea background noise sources obey Gaussian distributions. A Gaussian amplitude distribution does not provide a good fit to the observed 3–5.6 μm sea background data and the 8–14 μm clear sky background. Scene contamination may have caused the 3–5.6 μm sea background to deviate from a Gaussian distribution. In addition, the amplitudes of the 8–14 μm clear sky background fall into the non–linear portion of the dynamic range of the scanner. As a result, no conclusion is made regarding the parent distributions for 3–5.6 μm sea background or the 8–14 μm clear sky background.

C.1

TABLE OF CONTENTS

ACKNOWLEDGEMENTS

This work was sponsored by the Naval Environmental Prediction Research Facility and the Naval Postgraduate School. The assistance of Professor A. W. Cooper was much appreciated. His careful proofreading of this thesis was invaluable. The author also would like to acknowledge the technical assistance provided by Mrs. Mary Atchley and Mr. Bob Sanders. In addition, Professor E. Milne provided generous assistance,time, and information.

Finally, the author's most sincere gratitude is extended to Professor David D. Cleary whose guidance made this work complete.

I. INTRODUCTION

A. GENERAL

During recent years, a large number of sophisticated Infrared detection systems have been investigated and developed. In an Infrared detection system it is necessary to suppress background noise to detect the target. The suppression of infrared backgrounds for the purpose of target detection requires a knowledge of the statistical metrics of the amplitude distribution. Specifically the mean, variance, and parent distribution must be known for each type of background.

In 1974, Itakura et al [Ref. 1] presented the results of a statistical analysis of IR backgrounds obtained with a radiometer over the wavelength range from 2 to 14 μm. Statistical properties of sky–, forest– and cities–backgrounds were described in this study. The background noise was described as a set of random two–dimensional pulses. The results showed the amplitude distribution of background spatial radiance, for thermal radiation emitted between 8–14 μm, obeyed Gaussian statistics whereas in the spectral region dominated by scattered sunlight (2–3 μm) the amplitude distribution followed Poisson statistics. The pulse width was described by a Poisson distribution.

Manolopoulos [Ref. 2] measured the radiance of several objects with an AGEMA THV 780 infrared scanner. The purpose of this study was to provide background radiance values for the development of the AN/SAR–8 Infrared Search and Target Designation (IRSTD) system. In order to validate the Schwartz–Hon (SH) model of the sea surface emissivity and the sky radiance incident (or reflected)

on the sea, thermal images of the sky and the sea background radiance were analyzed by Psihogios [Ref. 3] with the same thermal imaging system. Although both of these investigations used the AGEMA THV 780, they did not perform an indepth statistical analysis of background amplitude distributions.

B. PURPOSE AND ORGANIZATION OF THESIS

The purpose of this study is to describe the amplitude distribution of backgrounds which were not studied by Itakura et al. [Ref. 1]. The backgrounds investigated here include clear sky (3–5.6 μm and 8–14 μm), overcast sky (3–5.6 μm), and sea surface (3–5.6 μm and 8–14 μm). No attempt was made to investigate the spatial frequency of background noise.

The present work consists of five chapters including the introduction. The thesis is organized as follows:

* Chapter I is the Introduction.
* Chapter II is an overview of the subjects considered during this study such as thermal radiation laws and statistical methods.
* Chapter III describes the equipment and the techniques of measurement.
* Chapter IV presents a description of the measurements and the results of the data analysis.
* Chapter V discusses the results of chapter IV and presents recommendations for further studies in this area.
* Appendixes A and B show the listing of FORTRAN programs SB1 and SB2, respectively.
* Appendix C describes the transfer procedure of the thermal image data collected using an if800 microcomputer.

II. BACKGROUND TO PROBLEM

A. IR RADIATION AND THERMAL IMAGING

All non–target objects which scatter, reflect, or emit infrared radiation are considered background noise sources. Examples include the sun, clouds, land, sea, sky and birds. Measurement of the background noise can be done using a "Thermal Imaging System". Thermal imaging systems are thoroughly described by Lloyd [Ref. 4].

Four wavelength regions of the IR spectrum can be used in IR imaging. These include the near infrared region with wavelengths of about 1 μm and other windows at 2–2.5 μm, 3–5.6 μm, and 8–14 μm. Detection in other parts of the spectrum is restricted by atmospheric absorption by water and carbon dioxide molecules (see Figure 1). Imaging in all these regions can be carried out with ambient or active illumination. For wavelengths greater than 3 μm, the object's black body thermal radiation is sufficient for thermal imaging. However, the contrast of thermal imaging is very low, particularly in the 8–12 μm portion of the spectrum where most of the thermal radiation energy is concentrated. Since a thermal resolution of 0.1 K is typically sought with background at 300 K, the uniformity requirements of image sensor responsivity in this region are very severe. [Ref. 5].

The "AGA 780 Thermovision", which was used to collect the data, is a liquid nitrogen cooled thermographic device able to detect IR radiation in the Middle IR, ($3 - 5.6$ μm designated SW by AGEMA), and in the Far IR, ($8 - 14$ μm designated LW) regions. Although these bandwidths do not coincide with the atmospheric window shown in Fig. 1, the overlap is considered sufficient.

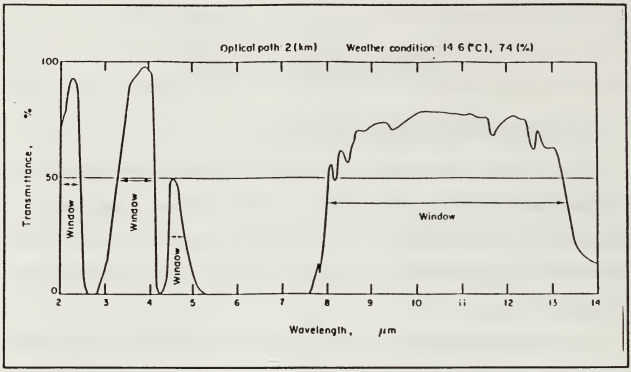

Figure 1. Spectral Transmittance of the Atmosphere (Reproduced from Ref. 1)

B. THERMAL RADIATION LAWS

In 1860 Kirchhoff introduced the law that states, in effect, that good absorbers are also good radiators. He also proposed the term *blackbody* to describe a body that absorbs all of the incident radiant energy and that, as a consequence of his law, must also be the most efficient radiator. In 1900 Planck described the spectral distribution of the radiation from a blackbody as

$$W_\lambda = \frac{c_1}{\lambda^5 \left(e^{c_2/\lambda T} - 1\right)}, \qquad (2-1)$$

where W_λ is the spectral emittance, W $cm^{-2}\mu m^{-1}$, λ is wavelength, μm, T is the absolute temperature, K, c_1 is the first radiation constant equal to $3.7415 \times 10^4 \pm 0.0003$ W $cm^{-2}\mu m^4$ and c_2 is the second radiation constant equal to $1.38054 \pm 0.00018 \times 10^{-4}$ W sec K^{-1}. [Ref. 6].

Planck's law can also be written in terms of photon cm^{-2} sec^{-1} μm^{-1} by dividing Eqn. $2-1$ by hc/λ, which is the energy associated with one photon, giving

$$Q = \frac{c_1'}{\lambda^4 \left(e^{c_2/\lambda T} - 1\right)}, \qquad (2-2)$$

where Q is the spectral radiant photon emittance, photon sec^{-1} cm^{-2}, and c_1' is a constant equal to 1.88365×10^{23} sec^{-1} cm^{-2} μm^3. [Ref 6].

Figure 2, which is reproduced from Ref. 6, shows the spectral radiant emittance of a blackbody at various temperatures, ranging from 500°K to 900°K.

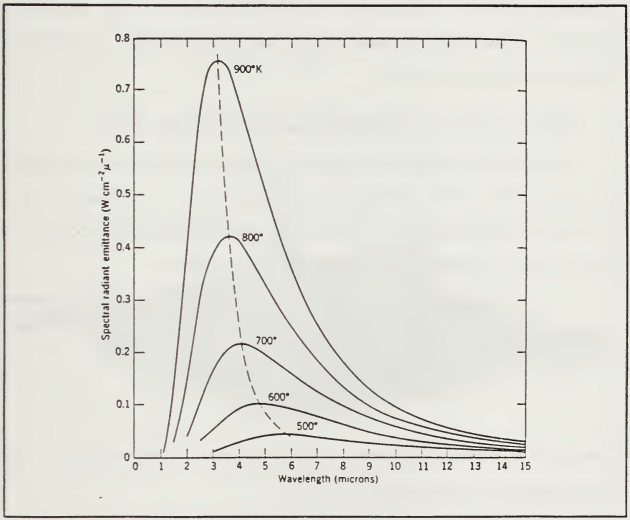

Figure 2. Spectral Radiant Emittance of a Blackbody

C. THE EFFECT OF BACKGROUND NOISE

The effect of the sea and sky background noise can be seen easily in Fig. 3. Figure 3(a) and Figure 3(b) are surface plots of the long wavelength image of an approaching ship. In Fig. 3(a), the peak created by the ship is hardly recognizable on the intersection line of the sea and the sky background and the signal–to–noise ratio is obviously small. In Fig. 3(b) the target is closer and easily distinguishable; the signal–to–noise ratio is also improved.

It is seen clearly that the amplitude of the sky background noise is higher than the sea background noise because the temperature of the sky is higher than the temperature of the sea. Whenever the temperature of either sea or sky changes, the amplitude of the noise fluctuations will also change without changing the distribution function of the noise.

D. THE STATISTICAL MODEL OF THE BACKGROUND NOISE

The statistical properties of infrared background noise have been analyzed previously [Ref. 1]. The statistical model developed was a random set of two–dimensional pulses whose amplitudes obey either Gaussian distributions in the 8–14 μm region or Poisson distributions in the 2–3 μm region.

It is assumed that the radiance received by the system obeys Gaussian statistics in both the 3–5.6 μm and 8–14 μm region, as follows;

$$p_g(n) = \frac{1}{\sqrt{2\pi\sigma^2}} e^{-(n-\bar{n})^2/2\sigma^2}, \qquad (2-3)$$

where p_g is a Gaussian distribution; n is the radiance of a certain point, $\bar{n}$ is the average radiance, σ^2 is the variance of n.

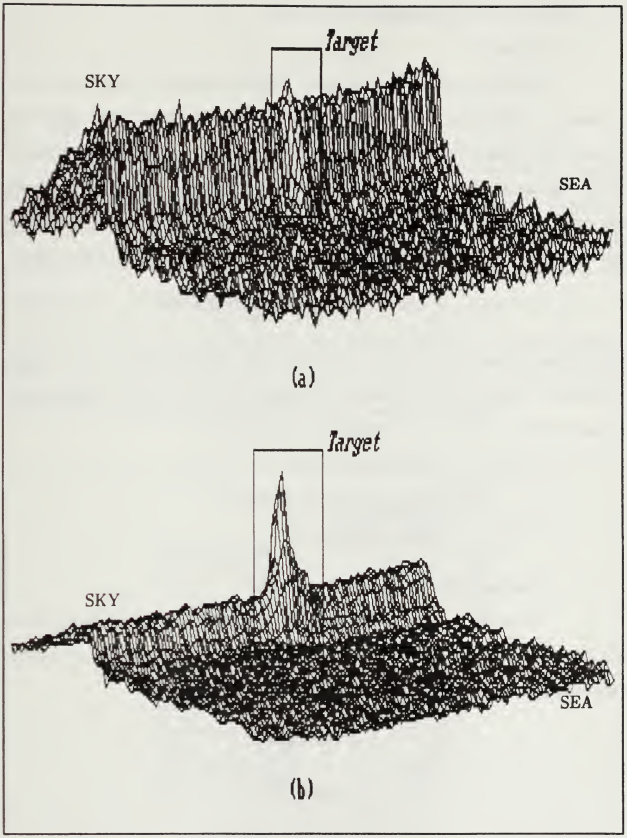

Figure 3. Surface Plot of Apparent Thermal Values (IU): (a) target is distant; (b) Target is close.

E. CHI–SQUARE GOODNESS OF FIT TEST

1. Procedure

In this investigation it is assumed that the background noise comes from a Gaussian distribution. The null hypothesis states that there is no difference between the expected and actual sample distributions. The null hypothesis is tested using a Chi–squared test. After obtaining each infrared image, the data are grouped into amplitude cells. The frequency–of–occurrence values have been compared with those expected under the null hypothesis. The test procedure uses χ^2 statistics given

$$\chi^2 = \sum_{i=1}^{k} \frac{(\text{observed} - \text{estimated expected})^2}{\text{estimated expected}}. \qquad (2-4)$$

This expression has approximately a chi–square distribution with $k-1-m$ degrees of freedom, whereby k is the number of cells, m is the number of parameters estimated [Ref. 7]. The test procedure used in this study is:

* if $\chi^2 \leq \chi^2_{.01,k-1-m}$, accept null hypothesis
* if $\chi^2_{.01,k-1-m} < \chi^2 \leq \chi^2_{.005,k-1-m}$, withhold judgment
* if $\chi^2 > \chi^2_{.005,k-1-m}$, reject null hypothesis

2. Goodness of Fit for Normal Distribution

If the null hypothesis states that the underlying distribution is normal, the χ^2 test must be preceded by a choice of cell size and an estimation of the mean value and standard deviation. These are determined using

$$\hat{\mu} = \bar{n} = \frac{\Sigma n_j}{N}, \qquad (2-5)$$

$$\hat{\sigma} = \left[\frac{\Sigma(n_j - \bar{n})^2}{N}\right]^{1/2}, \qquad (2-6)$$

where n_j is the radiance of point j, $\bar{n}$ is the average radiance and N is the sample size. The number of parameters estimated is two and hence m=2. [Ref. 7].

III. EQUIPMENT

A. THE AGA THERMOVISION SYSTEM

In this study an AGA 780 Thermovision Thermal Imaging system was used as measurement equipment. The Thermovision 780 system, a fourth generation development of "AGA Thermovision" which was first introduced in 1965, is designed for both image recording and image analysis. The basic Thermovision 780 system [Fig. 4] consists of a Black/White monitor chassis together with the dual scanner unit [Ref. 8]. In addition to this basic system, the Thermovision 780 System used in this study also includes a Sony RGB color monitor and an IBM AT microcomputer configured with AGEMA system cards and software.

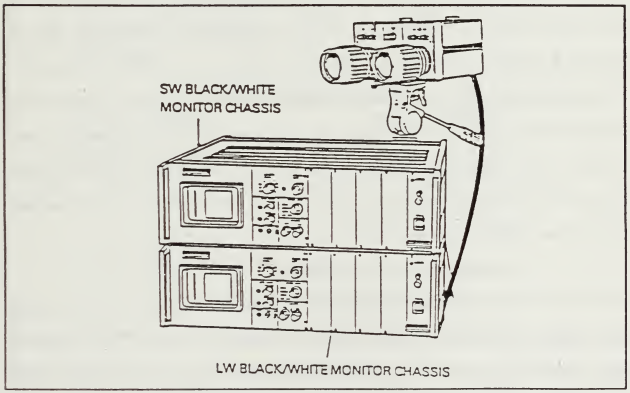

Figure 4. The Basic Thermovision 780 System

B. BASIC DESCRIPTION OF THE SYSTEM UNITS

1. The Dual Scanner Unit

This unit consists of two serial scanning cameras each containing a single detector. One camera covers the 3 to 5.6 μm spectral band (SW) and the other covers the 8 to 14 μm spectral band (LW). The cameras convert electromagnetic thermal energy radiated from an object into electronic video signals which are amplified and transmitted via an interconnecting cable to the Black/White monitor chassis. [Ref. 7].

a. Electro–Optical Scanning Mechanism

The two bands of the scanner use separate optics, which make it possible to cover both the long and short wavelength simultaneously. Two rotating refractive prisms with eight sides, one on the vertical axis and one on the horizontal axis, are used to scan the scene in a raster pattern. The synchronized rotation of horizontal and vertical prisms provides 100 horizontal scanning lines, with four to one interlace producing 400 lines per frame. The lenses of the system are made of germanium for LW and silicon for SW with 7^0 fields of view. The lenses can be focused in the same way as normal photographic lenses. The aperture stop can be adjusted between f/1.8 and f/20 and is controlled from the front of the scanner unit. Another control on the front of the scanner allows the selection of a specific filter. The data has been collected using lenses with a 7^0 field of view, the f/1.8 aperture stop and the unfiltered position. [Ref. 8].

b. Infrared Detectors and Cooling

An Indium–Antimonide (InSb) detector in the 3 to 5.6 μm band and a Mercury–Cadmium–Telluride (HgCdTe) detector in the 8 to 14 μm band are used. Both are single element point detectors and are cooled to -196^0C using liquid nitrogen. [Ref. 8].

c. *Technical Data*

Technical data for the dual AGA 780 scanner is reproduced from Ref. 8 and Ref. 9 and shown in Table 1.

Table 1. AGA 780 TECHNICAL DATA

Performance Characteristics			
Spectral Region (μm)		:	5.6 and/or 8 – 14
Spectral rate (Sec^{-1})		:	6.25
Field rate (Sec^{-1})		:	25
Interlace		:	4 to 1
Replaceable Fore–Optics			
FOV (deg.)	AZ	:	7.0
	EL	:	7.0
IFOV (mrad.)	AZ	:	1.1
	El	:	1.1
NEΔT at 22°C	(°C)	:	0.12
MDT	(°C)	:	< 0.1
Dynamic Range	(°C)	:	– 20 to 900
Optical Data			
Effective Aperture Area (cm^2)		:	24.0
Diameter of Aperture (cm)		:	5.5
Effective Focal Length (cm)		:	9.9
f/ number		:	1.8
Detector and Cooler Data			
Type of Material		:	InSb or HgCdTe
Number of Elements		:	1
Peak Wavelength		:	5 or 10
Cooler Type		:	liquid nitrogen

2. The Black/White Monitor Chassis

The video signal from the scanner unit is amplified and processed within the monitor chassis and applied to the display screen. The monitor chassis also supplies the required sweep signals, isotherms, and power supply. Output from this unit is connected to the IBM AT microcomputer via appropriate interface cable.

The Black/White monitor screen, which displays the 280 lines of 400 lines per frame, is covered by a mask [Fig. 5] with vertical and horizontal scales which are illuminated by the display raster. The horizontal numbers at the top of the screen show the Thermal Range setting, from 2 to 1000. The vertical scale, graduated –0.5 to +0.5, corresponds to the fraction of the range selected. [Ref. 8].

Table 2 describes the operation of the controls associated with the conversion from isotherm units to radiance and Figure 6, reproduced from Ref. 8, shows the controls and indicators on the front panel of B/W monitor chassis.

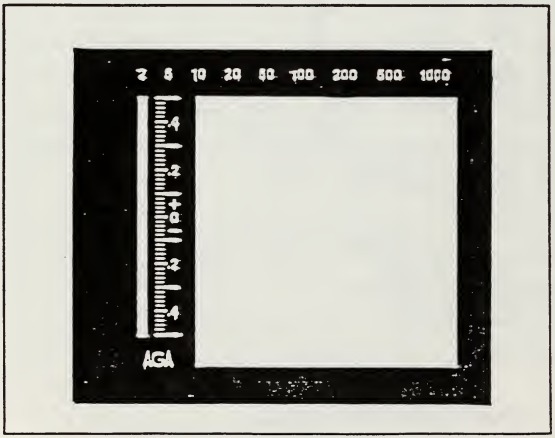

Figure 5. B/W Monitor Screen Mask

Table 2. BLACK/WHITE MONITOR CHASSIS
SELECTED FRONT PANEL CONTROLS

Item	Description	Function
1	POWER	This push ON/OFF button controls the ac supply to the THV 780 system.
9	THERMAL RANGE	This nine position switch selects the thermal span of interest. The switch is calibrated between 2 and 100 IU.
10	THERMAL LEVEL	This control sets the thermal level of the thermal image.
11	THERMAL L. ADJ	This control provides fine adjusment for calibration of the thermal level

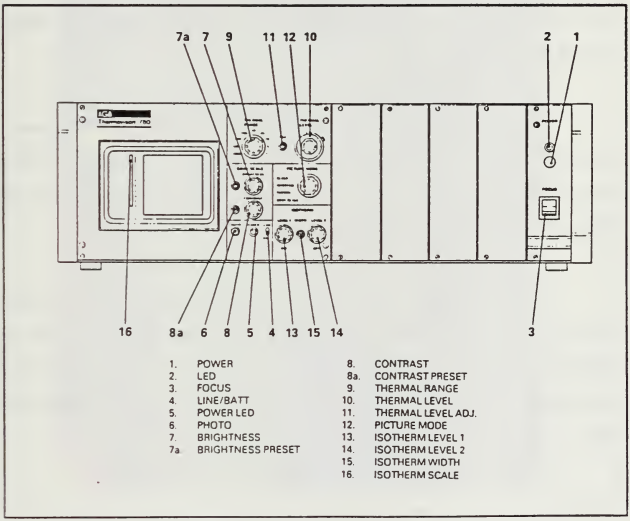

Figure 6. Black/White Monitor Chassis Controls and Indicators

3. The IBM AT Microcomputer

An IBM AT computer is configured with AGEMA system cards and software in order to build the Thermal Image Computer (TIC–8000). This TIC–8000 has menu–directed AGEMA software and works with the MS–DOS operating system [Ref. 10]. Previously, the BMC if800 microcomputer, DISCON scan converter and IR–Link had been used for the same purposes. The TIC–8000 makes possible live mode image display and processing as well as storing the data into binary files which can be accessed easily. The TIC–8000 with RGB monitor and Cannon color printer has been used for the initial analysis and digital recording of data. Unfortunately, there exists a problem in the current configuration. RANGE and LEVEL do not transfer to the TIC–8000 automatically. They must be entered by hand for each stored image.

a. Digital Image

The amplified analog video signal from the B/W monitor chassis is converted to an 8 bit digital signal with the full binary range of 256. The 140x140 pixel element matrix from a single vertical scan is processed in real time and displayed on the RGB monitor [Fig. 7].

b. Data File Structure

The image can be stored into the image sub directory as a binary file with a record length 20446 bytes where the image data starts at byte 846. The 140x140 pixel element matrix is stored in such a way that the even numbered lines are stored in the first 9800 bytes and the odd numbered lines in the second 9800 bytes.

Figure 7. The TIC–8000 Screen with The 140x140 Pixel Digital Image

C. MEASUREMENT TECHNIQUES

The AGA THV 780 infrared scanner measures the scene radiance and stores the result in Isotherm Units (IU) which is a arbitrary unit of measurement. The detected radiance for a given pixel is assigned a thermal value. The thermal value is proportional to the received photon radiation and is related to the blackbody temperature through a nonlinear curve defined by individual calibration constants. [Ref. 8].

The two basic methods of measuring the temperature by using AGA THV 780, direct measurement and relative measurement, are thoroughly described in Ref. 8. The direct measurement technique has been used to measure the scene radiance in this study.

1. Direct Measurement

The equipment is used to obtain the scene radiance directly without the use of an external reference source of radiation. The thermal value is set by the values of the "Thermal Level" and "Thermal Range" knobs on the B/W monitor chassis where the thermal range sets the dynamic range of the scanner and the thermal level sets the median value of thermal value to which the scanner responds. After adjusting the "Thermal Level" and "Thermal Range" controls to get a satisfactory picture and the "Isotherm Level 1" control to highlight the point of interest, the marker reading of isotherm scale is multiplied by the "Thermal Range" setting and added to the "Thermal Level" setting. The result is the measured thermal value in Isotherm Units (IU) which represents the scene radiance [Fig. 8] or alternatively the scene radiant emittance. Assuming the object is a blackbody and is positioned at a distance of one meter from the scanner, the calibration function can be used directly to find temperature [Ref. 8].

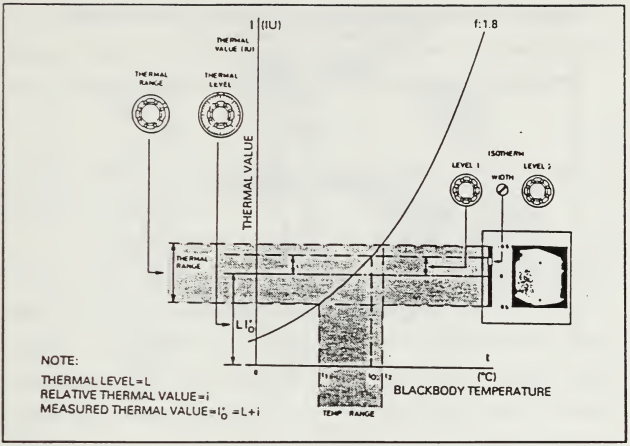

Figure 8. Direct Temperature Measurement Procedure [Ref. 8]

2. Calibration Functions

The calibration curves used to convert measured thermal value to object temperature are described by the mathematical model:

$$I = \frac{A}{C\ e^{B/T} - 1} \quad . \qquad (3-1)$$

Here I is the thermal value, T is the absolute temperature (K) and A,B,C are factory calibration constants. The individual calibration data is given in Table 3 and the calibration curves are illustrated in Figure 9. [Ref. 8].

Table 3. INDIVIDUAL CALIBRATION OF 780 DUAL SCANNER
(Reproduced from Ref. 8)

SERIAL NUMBERS		
SCANNER	: SWDB 4011	LWDB 4011
DETECTOR	: G 1739	G 1739
FILTER	: NOF	NOF
LENS	: 7 3009	7 3105
CALIBRATION CONDITIONS		
AMBIENT TEMPERATURE	: 23 °C	24 °C
RELATIVE HUMIDITY	: 50 %	55 %
OBJECTIVE DISTANCE	: 1.0 m	1.0 m
CALIBRATION DATE	: 82-09-17	82-09-27
OPERATOR	: B.A	B.A
CALIBRATION CURVE CONSTANTS		
A	: 811203	-3581
B	: 3117.74	1506.49
C	: 1.00	-0.436

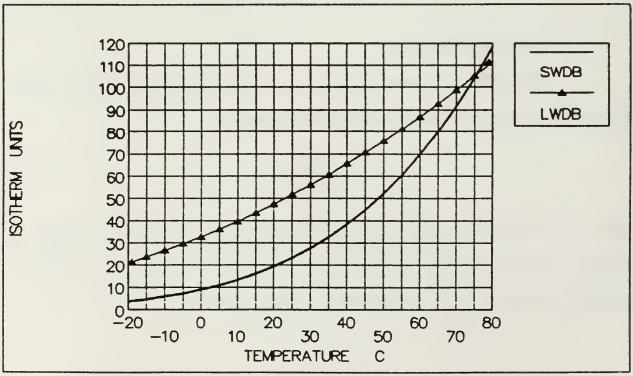

Figure 9. SW and LW Calibration Curves (−20 °C to 80 °C)

Because thermal value is a non–standard quantity, the images are converted to values of radiant emittance. There exists a linear relationship between thermal value and radiant emittance [Ref. 8]. This relationship can be written as

$$W = m \cdot [I + c] \qquad (3-2)$$

where W is radiant emittance (W cm^{-2}), I is thermal value (IU), and m and c are individual calibration factors.

The radiant emittance can be calculated directly from the Eq. 3–2 once m and c have been determined. In order to determine these constants, a FORTRAN program called SB1 has been written (listing of this program appears in Appendix A). The program first calculates the temperature from the thermal value using equation 3–1. These temperatures are then used to calculate radiant emittance by integrating Planck' Law over the specified spectral region. The results of SB1 are shown in Figures 10 and 11 for SW and LW, respectively. The linear relationship between radiant emittance and thermal value can easily be observed in both Figures. By using a simple linear computation, these relationships were defined as

$$W = 4.69 \times 10^{-5} \cdot [I + 1] \quad \text{for SW} \qquad (3-3)$$

and

$$W = 3.03 \times 10^{-4} \cdot [I + 3.624] \quad \text{for LW.} \qquad (3-4)$$

Thus, the parameters of Eq. (3 – 2), m and c, are respectively 4.69×10^{-5} (W cm^{-2} IU^{-1}) and 1 (IU) for SW, 3.03×10^{-4} (W cm^{-2} IU^{-1}) and 3.624 (IU) for LW.

These calibration constants assume an object distance of one meter. Because the distances of the background noise sources are poorly defined, an apparent radiant emittance is introduced. The apparent radiant emittance is defined here as the radiant emittance of a blackbody at a distance of one meter

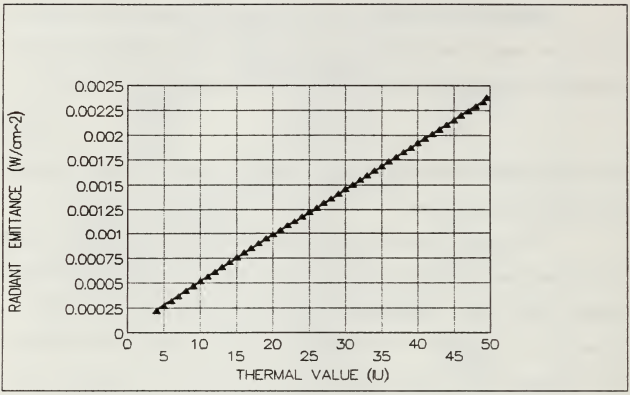

Figure 10. SB1 Output for SW (4 IU to 50 IU)

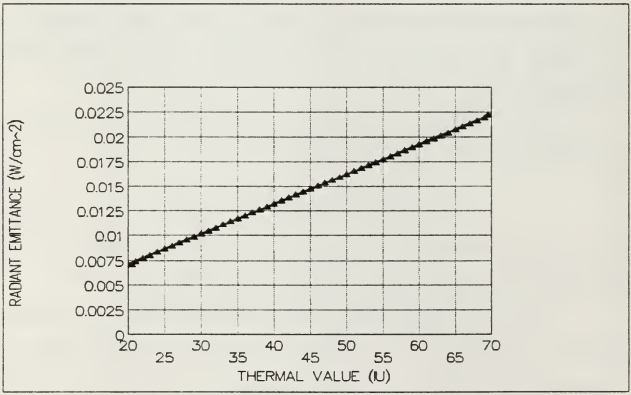

Figure 11. SB1 Output for LW (19 IU to 70 IU)

IV. MEASUREMENTS AND DATA ANALYSIS

A. MEASUREMENTS

The measurements were made from the roof of Building 232 (Spanagel Hall) of the Naval Postgraduate School and from Hopkins Marine Station. The measurements from the roof of Spanagel Hall were made between 12 and 4 o'clock P.M.. In addition, images of the LW sea surface were taken during Nov, 1988, from the Moss Landing Marine Lab [Ref. 3]. These images were transferred from the if800 computer to the IBM–AT computer using the DISPORT transfer program (the description of the image transfer procedure appears in Appendix C.). Table 4 shows the list of measured objects with initial measurement parameters.

Table 4. LIST OF MEASURED OBJECTS

Date	Band	# of Img.	Object	Air Tmp.	Weather	Az.El.
11.01.88	LW	30	Sea	19 ^{0}C	—	Random
11.05.88	LW	45	Sea	19 ^{0}C	—	Random
08.31.89	SW	19	Sky	20 ^{0}C	Clear	Random
09.01.89	SW	08	Sky	19 ^{0}C	Cloudy	Random
09.05.89	SW	10	Sky	20 ^{0}C	Clear	SE,45^0
09.05.89	SW	05	Sky	20 ^{0}C	Clear	S ,70^0
09.05.89	SW	05	Sky	20 ^{0}C	Clear	SW,75^0
09.08.89	LW	20	Sky	19 C	Clear	Random
09.14.89	SW	20	Sea	18 C	—	Random
09.15.89	LW	20	Sky	21 C	—	Random

B. DATA ANALYSIS

1. Procedure

Because of the vignetting at edges of the field–of–view, during the data analysis only 40x40 pixels from the central part of the images were used. This reduced the FOV to 2^0 and the instrument factor to a negligible level. This also reduced the sample size from 19600 to 1600.

Each sample value is converted to apparent radiant emittance (W cm^{-2}) from Isotherm Units (IU). A FORTRAN program called SB2 was written for this conversion (listing of this program appears in Appendix B). SB2 reads the image file and writes the output as apparent radiant emittance (W cm^{-2}) in the form of a 40x40 matrix. Then, each sample is converted to the radiance as a string of 1600 values. Images recorded with the original if800 system were reduced using somewhat smaller sample sizes to cover only sea surface.

In the analysis of these quantitative sample values, the first set of calculations of basic statistics were performed by using the STATGRAPHICS program (Statgraphics is a registered trademark of Statistical Graphics Corporation). These calculations are

* average
* variance
* standard deviation
* geometric mean
* minimum, maximum and range
* standard error
* standardized skewness and standardized kurtosis
* median
* mode

The standardized coefficients show the deviations from the normal distribution while the average, median, mode and geometric mean measure the central tendency and standard deviation, range and variance measure spread of the data. [Ref. 11]

After initial analysis, the samples were normalized and a Chi–square test was conducted. The results are presented in the following sections while these results are discussed in the next Chapter.

2. **Analysis Of Sky Background Noise**

a. SW – Clear Sky

A total 39 images of the SW clear sky have been analyzed. These images were taken from the roof of Spanagel Hall at the Naval Postgraduate School, Monterey, Ca. during August and September, 1989.The first 19 images were recorded with a randomly selected scanner direction. The scanner direction during the recording of the last twenty images was selected in such a way to examine the effect of the scattered sunlight on the distribution type. This was done by choosing a portion of sky with strong sunlight influence.

A plot of the amplitude distribution for all 39 images is shown in Figure 12. The three features seen in this figure are due to differences in the mean amplitude. This variation of the mean is primarily due to changes in the azimuth and elevation of the viewing direction (see Table 4). As a result of the scatter in the data seen in this Figure, the mean value of each image was subtracted from the data producing normalized amplitudes (μ=0). The results are shown in Figure 13. The full Normalized sample values (with $\mu = 0$ and $\sigma = 1$) are shown in figure 14. Figure 15 shows the histogram of sample values from an image data and the standard Normal distribution.

The Chi–square test was conducted for each individual image as well as the overall data set under the null hypothesis that the underlying distribution was Normal. In order to test this the 12 cells with a width of 0.5 were chosen. The Chi–square values, observed and expected cell counts are listed in Table 5 for the overall data set. The computed χ^2 is 15.53218. The tabulated Chi–square for $k = 12$, and $m = 2$, and a significance level of 0.05 is $\chi^2_{.05;9} = 16.919$. (Recall from Chapter 2, k–1–m is the degrees of freedom, k is the number of cells, m is the number of parameters estimated.) Since 15.532 is less than 16.919, a normal distribution provides an excellent fit to the data. Observed and expected cell counts are illustrated in Figure 16. Table 6 shows the analysis results of the SW clear sky.

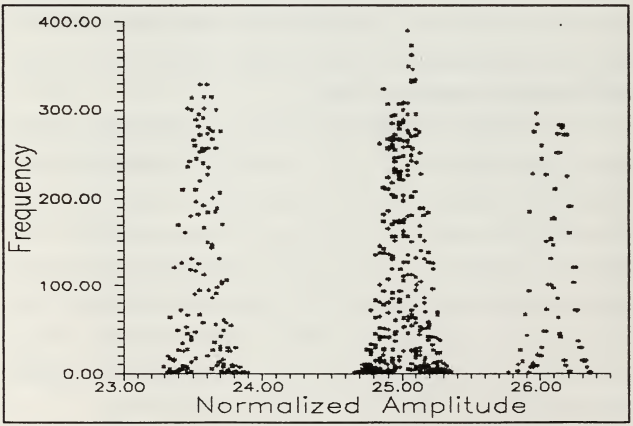

Figure 12. The Scatter Plot of Sample Values of SW Cl. Sky (10^{-5} W cm^{-2} sr^{-1})

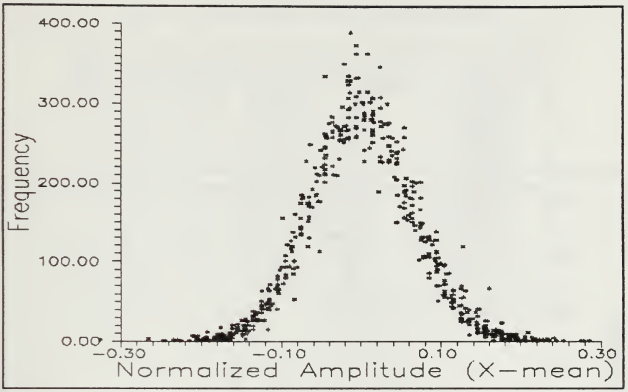

Figure 13. The Scatter Plot of Sample Values With Zero Mean (SW Clear Sky)

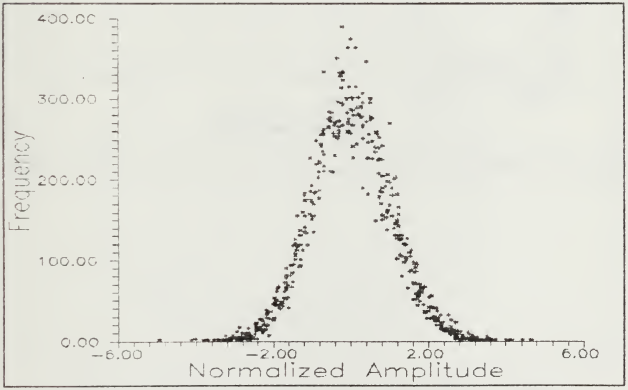

Figure 14. The Plot of Normalized Sample Values (SW Cl. Sky, $\mu = 0$ and $\sigma = 1$)

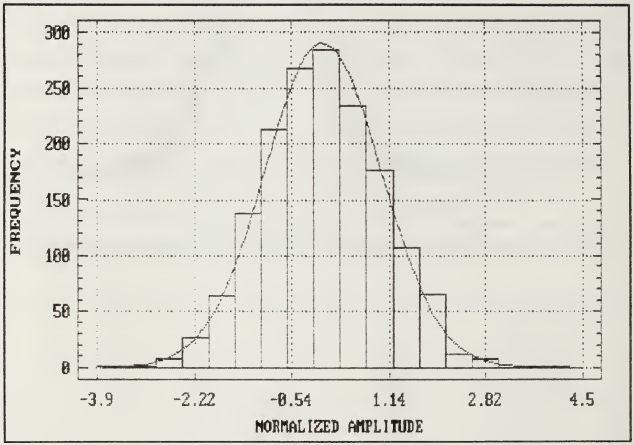

Figure 15. Standard Normal Distribution and Histogram of a Sample (SW CL. Sky)

Table 5. CHI–SQUARE TEST (SW CLEAR SKY)

Cell Num.	Lower Limit	Upper Limit	Observed Cell Count	Expected Cell Count	Chi-square Test Values
1	≤	-2.5	9.2450	9.9	0.043336
2	-2.5	-2.0	22.9745	26.5	0.469008
3	-2.0	-1.5	61.8166	70.5	1.069507
4	-1.5	-1.0	132.7684	147.0	1.377809
5	-1.0	-0.5	253.8439	239.8	0.822478
6	-0.5	0	355.0097	306.3	7.7460999
7	0	0.5	290.3175	306.3	0.8339499
8	0.5	1.0	215.2746	239.8	2.508327
9	1.0	1.5	146.5009	147.0	0.001695
10	1.5	2.0	72.1412	70.5	0.038208
11	2.0	2.5	27.8728	26.5	0.071117
12	2.5	<	12.2348	9.9	0.550651
k=12, m=2, k-m-1=9				Chi-square = 15.53218	

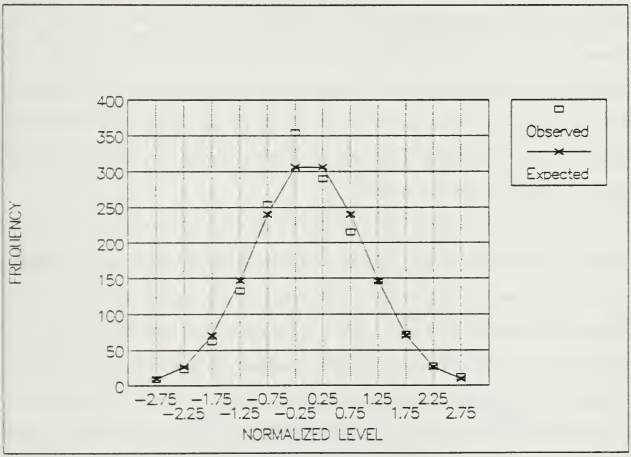

Figure 16. Observed and Expected Cell Counts (SW Clear Sky)

Table 6. THE RESULTS OF SW – CLEAR SKY ANALYSIS

Average	:	25.2716×10^{-5}	W cm^{-2} sr^{-1}
Variance	:	0.4	$(\mu W\ cm^{-2}\ sr^{-1})^2$
Standard dev.	:	0.63	$\mu W\ cm^{-2}\ sr^{-1}$
Minimum	:	23.29×10^{-5}	W cm^{-2} sr^{-1}
Maximum	:	30.3×10^{-5}	W cm^{-2} sr^{-1}
Range	:	7.01×10^{-5}	W cm^{-2} sr^{-1}
Average Range	:	0.41×10^{-5}	W cm^{-2} sr^{-1}

Goodness of Fit

Number of Samples	:	39	
Sig. Level ≥ 0.01	:	16	41%
Sig. Leel ≥ 0.005	:	19	48%

b. SW – Cloudy Sky

A total of 8 images of the SW cloudy sky were analyzed. The first 6 images were recorded randomly from overcast sky with high altitude clouds. Two images were recorded from 80% cloudy sky with medium altitude clouds. The purpose of recording these last two images was to see the effect of the two different kinds of background noise sources on the amplitude distribution. The normalized sample values from the 80% cloudy sky are shown in Figure 17. A discussion of this figure is deferred to the next chapter.

The normalized sample values from the overcast sky are shown in Figure 18.The Chi–squared test was conducted under the same null hypothesis described in the previous section. The computed Chi–square is 17.34588. The tabulated Chi–square for $k = 12$, $m = 2$ and a significance level of 0.025 is $\chi^2_{.025,9} =$ 19.022. Since 17.34588 is less than 19.022, a normal distribution provides a good fit to data. The observed and expected cell counts are listed in Table 7 and illustrated in Figure 19. Table 8 shows the analysis results of the SW samples of the overcast sky.

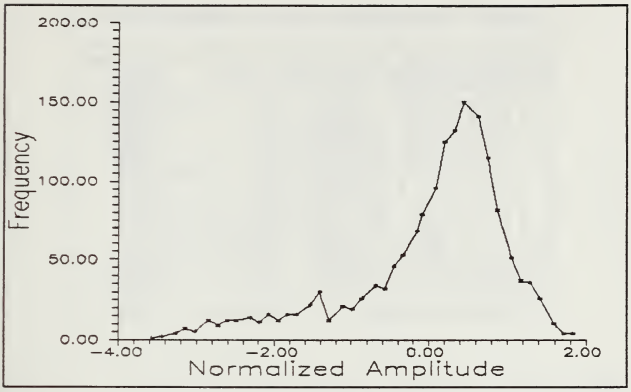

Figure 17. Normalized Sample Values of 80% Cloudy Sky ($\mu = 0$ and $\sigma = 1$)

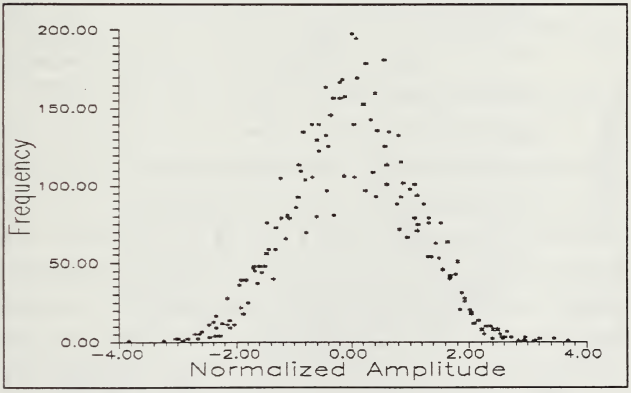

Figure 18. Normalized Sample Values of Overcast Sky ($\mu = 0$ and $\sigma = 1$)

Table 7. CHI–SQUARE TEST (SW OVERCAST SKY)

Cell Num.	Lower Limit	Upper Limit	Observed Cell Count	Expected Cell Count	Chi-square Test Values
1	<	-2.5	4.6667	9.9	2.766442
2	-2.5	-2.0	24.3333	26.5	0.177149
3	-2.0	-1.5	82.6667	70.5	2.099685
4	-1.5	-1.0	142.1667	147.0	0.158919
5	-1.0	-0.5	238.5000	239.8	0.001046
6	-0.5	0	310.0000	306.3	0.052288
7	0	0.5	280.1667	306.3	2.180919
8	0.5	1.0	238.1667	239.8	0.002906
9	1.0	1.5	155.3333	147.0	0.472411
10	1.5	2.0	93.6667	70.5	7.612687
11	2.0	2.5	24.5000	26.5	0.150943
12	2.5	<	5.83333	9.9	1.670483
k=12, m=2, k-m-1=9				Chi-square = 17.34588	

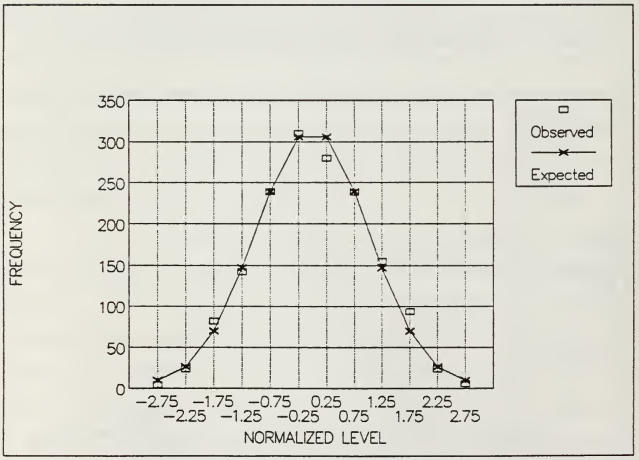

Figure 19. Observed and Expected Cell Counts (SW Overcast Sky)

Table 8. THE RESULTS OF SW – OVERCAST SKY ANALYSIS

Average	:	28.95×10^{-5}	W cm^{-2} sr^{-1}
Variance	:	1.75	$(\mu W\ cm^{-2}\ sr^{-1})^2$
Standard dev.	:	1.34	$\mu W\ cm^{-2}\ sr^{-1}$
Minimum	:	25.40×10^{-5}	W cm^{-2} sr^{-1}
Maximum	:	35.73×10^{-5}	W cm^{-2} sr^{-1}
Range	:	10.33×10^{-5}	W cm^{-2} sr^{-1}
Average Range	:	0.78×10^{-5}	W cm^{-2} sr^{-1}

Goodness of Fit

Number of Samples	: 6	
Sig. Level ≥ 0.01	: 1	17%
Sig. Level ≥ 0.005	: 3	50%

c. LW – Clear Sky

A total of 30 images have been analyzed for the LW clear sky. Some of the images were recorded under a partly cloudy weather condition but the data were taken only from the clear part of the sky. The normalized sample values from these 30 images were shown in Figure 20. This normalized scatter plot indicates that the sample values are piled about the mean.

The result of the Chi–squre test showed that normal distribution did not provide a good fit to data under the null hypothesis described in the previous sections. The computed Chi–square is 174. The tabulated Chi–square for $k = 12$, $m = 2$ and a significance level of 0.005 is $\chi^2_{.005,9} = 23.587$. Since 174 is much more than 23.587, the null hypothesis is rejected. The deviation of observed cell counts from expected cell counts can be seen easily in Figure 21. None of the 30 samples individually fitted to normal distribution either. Table 9 shows the analysis results of the LW samples of the clear sky. The results of this section are discussed in the next chapter.

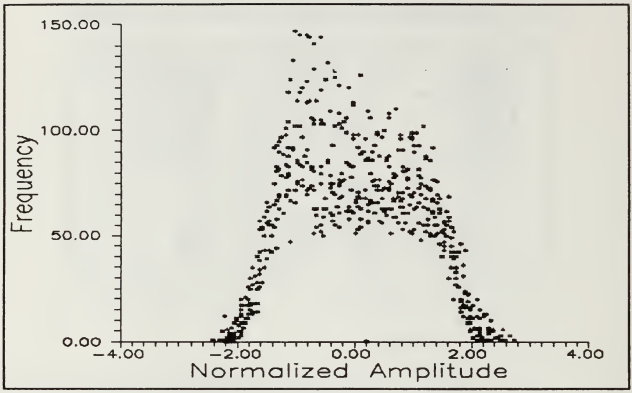

Figure 20.The Plot of Normalised Sample Values (LW Cl. Sky $\mu = 0$ and $\sigma = 1$)

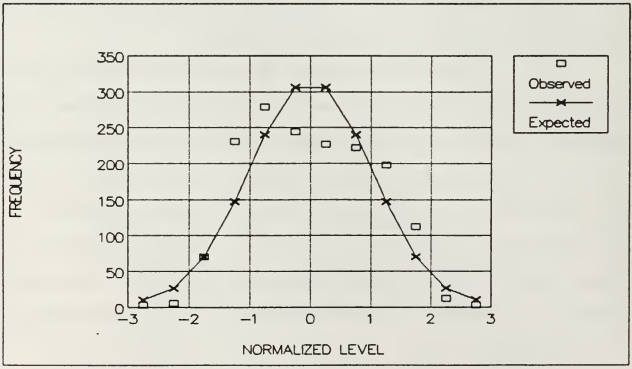

Figure 21. Observed and Expected Cell Counts (LW Clear Sky)

Table 9. THE RESULTS OF LW – CLEAR SKY ANALYSIS

Average	:	22.55×10^{-4}	W cm^{-2} sr^{-1}
Variance	:	1.21×10^{-10}	$(W\ cm^{-2}\ sr^{-1})^2$
Standard dev.	:	0.11×10^{-4}	W cm^{-2} sr^{-1}
Minimum	:	22.55×10^{-4}	W cm^{-2} sr^{-1}
Maximum	:	35.05×10^{-4}	W cm^{-2} sr^{-1}
Range	:	12.50×10^{-4}	W cm^{-2} sr^{-1}
Average Range	:	0.49×10^{-4}	W cm^{-2} sr^{-1}

Goodness of Fit

Number of Samples	:	30
Sig. Level ≥ 0.01	:	NONE
Sig. Level ≥ 0.005	:	NONE

3. Analysis Of Sea Background Noise

a. *SW – Sea Surface*

A total of 20 images have been analyzed for the SW sea surface. The images were taken from the Hopkins Marine Station on Sept. 14, 1989. Due to limitations in the field–of–view, the images included objects other than the sea surface. In order to cover only the sea surface, eight hundred pixels of image data were selected. The normalized sample values from these 20 images were shown in Figure 22.

The result of the Chi–square test showed that normal distribution did not provide a good fit to data for overall sample values. The computed Chi–square is 70.88. The tabulated Chi–square for $k = 12$, $m = 2$ and a significance level of 0.005 is $\chi^2_{.005,9} = 23.587$. Since 70.88 is much more than 23.587, the null hypothesis is rejected. The deviation of observed cell counts from expected cell counts can be seen in Figure 23. However, four samples fitted to a normal distribution individually. Table 10 shows the analysis results of the SW samples of the sea surface.

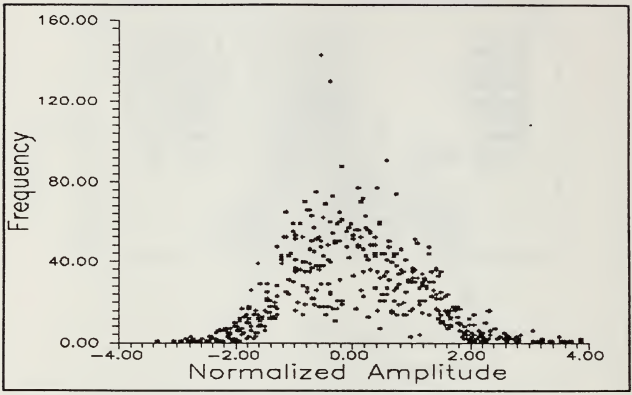

Figure 22.The Plot of Normalized Sample Values (SW Sea Surf., $\mu = 0$ and $\sigma = 1$)

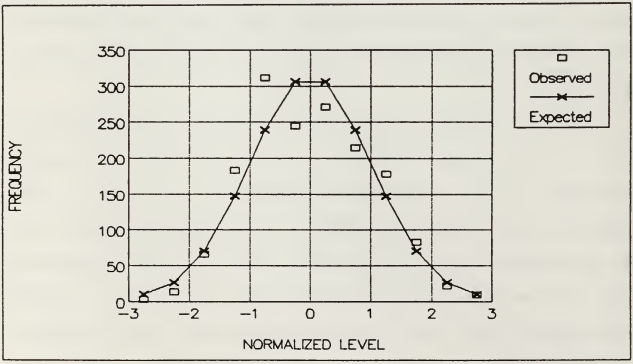

Figure 23. Observed and Expected Cell Counts (SW Sea Surface)

Table 10. THE RESULTS OF SW – SEA SURFACE ANALYSIS

Average	:	26.45×10^{-5}	W cm^{-2} sr^{-1}
Variance	:	5.27×10^{-13}	(W cm^{-2} sr^{-1})^2
Standard dev.	:	7.26×10^{-7}	W cm^{-2} sr^{-1}
Minimum	:	25.40×10^{-5}	W cm^{-2} sr^{-1}
Maximum	:	28.40×10^{-5}	W cm^{-2} sr^{-1}
Range	:	3.01×10^{-5}	W cm^{-2} sr^{-1}
Average Range	:	0.55×10^{-5}	W cm^{-2} sr^{-1}

Goodness of Fit

Number of Samples	:	20	
Sig. Level ≥ 0.01	:	4	20%
Sig. Level ≥ 0.005	:	5	25%

b. LW – Sea Surface

A total of 20 images of the LW sea surface were analyzed. The images were taken during November, 1988, from the Moss Landing Marine Lab [Ref. 2]. The sample size was reduced to 1279 in order to cover only sea surface. The normalized sample values from these 20 images were shown in Figure 24.

Chi–square values, and observed and estimated cell counts are listed in Table 11. The computed Chi–square is 22.75541. The tabulated Chi–square for $k = 12$, $m = 2$, and a significance level of 0.025 is $X^2_{.005,9} = 23.584$. Since 22.75 is less than 23.584, a normal distribution provides a good fit to the data. Observed and expected cell counts are also illustrated in Figure 25. Table 12 shows the analysis results of the LW samples.

Table 11. CHI–SQUARE TEST (LW SEA SURFACE)

Cell Num.	Lower Limit	Upper Limit	Observed Cell Count	Expected Cell Count	Chi-square Test Values
1	≤	−2.5	4.75	7.9	1.260884
2	−2.5	−2.0	11.95	21.17	4.013383
3	−2.0	−1.5	62.65	56.3	0.713381
4	−1.5	−1.0	132.45	117.4	1.928489
5	−1.0	−0.5	211.60	190.9	2.244293
6	−0.5	0	215.20	244.65	3.546687
7	0	0.5	267.05	244.65	2.049566
8	0.5	1.0	171.05	190.9	2.191969
9	1.0	1.5	103.60	117.4	1.625744
10	1.5	2.0	62.45	56.3	0.66907
11	2.0	2.5	24.25	21.17	0.449082
12	2.5	<	11.95	7.9	2.066646
k=12, m=2, k-m-1=9				Chi-square =	22.75541

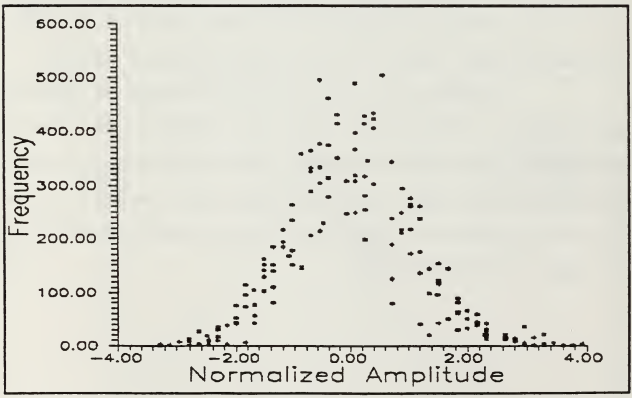

Figure 24.The Plot of Normalized Sample Values (LW Sea Surf., $\mu = 0$ and $\sigma = 1$)

Table 12. THE RESULTS OF LW – SEA SURFACE ANALYSIS

Average	:	43.00×10^{-4}	W cm^{-2} sr^{-1}
Variance	:	3.14×10^{-11}	$(W\ cm^{-2}\ sr^{-1})^2$
Standard dev.	:	0.56×10^{-5}	W cm^{-2} sr^{-1}
Minimum	:	42.75×10^{-4}	W cm^{-2} sr^{-1}
Maximum	:	43.30×10^{-4}	W cm^{-2} sr^{-1}
Range	:	0.55×10^{-4}	W cm^{-2} sr^{-1}
Average Range	:	0.33×10^{-4}	W cm^{-2} sr^{-1}

Goodness of Fit

Number of Samples	:	20	
Sig. Level $\geq$ 0.01	:	6	30%
Sig. Level $\geq$ 0.005	:	10	50%

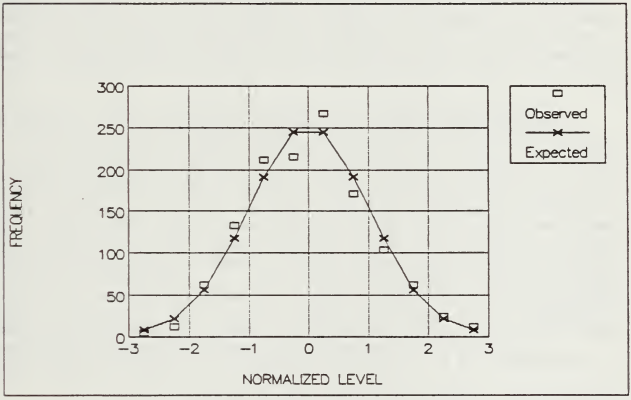

Figure 25. Observed and Expected Cell Counts (LW Sea Surface)

V. CONCLUSIONS AND RECOMMENDATIONS

A. CONCLUSIONS

The results presented in chapter IV show that the amplitude distributions of several infrared backgrounds in the spectral region 3–5.6 μm and 8–14 μm obey a normal distribution. In the 3–5.6 μm region, a normal distribution provides a good fit at the 0.05 level of significance for the clear sky background. The percentage of individual images obeying a normal distribution at the 0.01 level of significance is 41% and 48% at the 0.005 level of significance. The data show the mean amplitude varies with the viewing direction (Figure 12). However, the variance of the SW clear sky images does not change much. This can be seen by comparing Figures 13 and 14.

In the same spectral region, the overall data set for the overcast sky also fit a normal distribution at the 0.025 level of significance. One of the six images fitted a normal distribution at the 0.01 level of significance while three images fitted a normal distribution at the 0.005 level of significance. However, the distribution of the images containing both cloud and blue sky appears to deviate from a Gaussian [Fig. 17]. It is believed that this deviation is the result of a superposition of the two parent distributions. Based on the average amplitudes of the clear sky and overcast sky (see tables 6 and 8), it appears that the large peak in Fig. 17 is due to the overcast sky and "shoulder" on the left is due the clear sky.

In the 3–5.6 μm spectral region a normal distribution does not provide a good fit to the overall data set for the sea background. Due to limitations in the field–of–view, the images included objects other than the sea surface. This may

cause a deviation in the sample values from the normal distribution. Nevertheless, 20% of the sea surface images fit a normal distribution at the 0.01 level of significance and 25% of images fit a normal distribution at the 0.005 level of significance. This is clearly reflected in the overall amplitude distribution shown in Figure 23.

The amplitude distribution of the sea background in the spectral region 8–14 μm obeys a Gaussion distribution at the 0.005 level of significance. The percentage of individual images obeying a normal distribution is about 30% at the 0.01 level of significance and is about 50% at the 0.005 level of significance. The clear sky background in the spectral region 8–14 μm does not appear to obey a Gaussian distribution. The data collected from the clear sky, however, may not be valid because the amplitudes of the sample values from this band are very close to the lower end of the dynamic range of AGA THV 780 scanner. Due to this possible non–linearity, the measured sample values of LW–clear sky may be distorted.

The results of this investigation are summarized in Table 12. The amplitude distribution of the clear sky (3–5.6 μm), overcast sky (3–5,6 μm) and sea surface (8–14 μm) backgrounds can be described by Gaussian distribution. No conclusion is made regarding the parent distribution for the clear sky (8–14 μm) or the sea surface (3–5.6 μm) backgrounds.Where a sample set extends over two background types (eg cloud and clear sky) the distribution appears to be a bimodal one consisting of a superposition of the separate distributions for the two types.

Table 12. SUMMARY OF THE RESULTS

Background	3–5.6 μm Variance[1]	Distribution[2]	8–14 μm Variance	Distribution
Clear Sky	0.4×10^{-12}	Normal (0.05)	1.21×10^{-10}	Withhold Judgement
Overcast Sky	1.75×10^{-12}	Normal (0.025)	———	———
Sea Surface	0.53×10^{-12}	Withhold Judgement	3.14×10^{-11}	Normal (0.005)

[1] Unit: $(W\ cm^{-2}\ sr^{-1})^2$.
[2] Value in parenthesis indicates significance level.

B. RECOMMENDATIONS

Although the parent distributions of several important infrared backgrounds have been modeled with a Gaussian distribution, estimation of the mean and the standard deviation must be done very carefully to get the output of this modeling close to the real life values. In order to do this, the relationship between these two parameters and various background parameters, such as the air and the sea temperature, should be known. In general, the field–of–view will be composed of two or more background types. In this case, it is necessary to know the type and magnitude of the individual noise sources within a composite background. This requires further statistical analysis of the IR background noise parameters assuming the amplitude distribution is Gaussian.

APPENDIX A

LISTING OF THE SB1 FORTRAN PROGRAM

```
C     *******PURPOSE*******
C     THIS PROGRAM CALCULATES IN-BAND FLUX.
C     INPUTS:    LOWER AND UPPER LIMITS OF BAND
C                THE THERMAL VALUE (IU), OR TEMPERATURE IN K
C                OR °C
C                NUMBER OF INTERVALS
C     OUTPUT     W/cm², Photon/cm² vs IU
      INTEGER N,M,I,J,K,S,RET,BAL,DAL,YES,L,BIL
      REAL LAM,T(1000),ARA,A,G,C,Q(1000),U(1000),C1,C2,IX,
     +V4,W(1000),C3,LAM1,LAM2,DIV,TMAX,TMIN,TRAN,V1,V2,V3
      OPEN(UNIT=1, FILE='SONUC.TXT',
     +STATUS='UNKNOWN', ACCESS='SEQUENTIAL')
997   C1 = 37415
      C2 = 14387.9
      C3 = 188365
      IX = 1000
      IX = IX**6
      C3 = IX*C3
      PRINT *, ' ENTER WAVELENGTH1  (10xMICRONS)  '
      READ *, LAM1
      PRINT *, ' ENTER WAVELENGTH2  (10xMICRONS)  '
      READ *, LAM2
```

```
      PRINT *,'ENTER NUMBER OF INTERVALS OF THE INTEGRATION'
      READ *, DIV
      ARA = (LAM2–LAM1)/DIV
      WRITE(*,222) ara
222   FORMAT(3X,G15.8)
      IF(LAM1.LT.7) THEN
      A=811203
      G=3117.74
      C=1
      GOTO 2
      ENDIF
      A = –3581
      G = 1506.49
      C = –0.436
2     PRINT *, 'DO YOU USE TMV 780 UNITS'
      PRINT *, ' ENTER 1 FOR YES '
      PRINT *, ' ENTER 0 FOR NO '
      READ *, YES
      IF(YES.GT.0) GOTO 3
      PRINT *, ' WHAT IS THE INPUT UNIT? '
      PRINT *, ' ENTER 1 FOR TEMPERATURE IN KELVIN '
      PRINT *, ' ENTER 0 FOR TEMPERATURE IN CELCIUS'
      READ *, DAL
      IF(DAL.LT.1) THEN
      PRINT *, ' ENTER MIN TEMPERATURE IN CELCIUS'
      READ *, TMIN
```

```
      TMIN = TMIN+273
      PRINT *, ' ENTER MAX TEMPERATURE IN CELSIUS'
      READ *, TMAX
      TMAX = TMAX+273
      GO TO 1
      ENDIF
      PRINT *, ' ENTER MIN TEMPERATURE IN KELVIN'
      READ *, TMIN
      TMIN = TMIN
      PRINT *, ' ENTER MAX TEMPERATURE IN KELVIN'
      READ *, TMAX
      TMAX = TMAX
      GOTO 1
C-----------------------------------------------------------------
3     PRINT *, ' ENTER MIN ISOTHERM UNIT '
      READ *, TMIN
      TMIN = TMIN
      PRINT *, ' ENTER MAX ISOTHERM UNIT '
      READ *, TMAX
      TMAX = TMAX
C-----------------------------------------------------------------
1     TRAN = TMAX-TMIN
      K = INT(TRAN)
      K=K+1
      DIV = DIV+1
C-----------------------------------------------------------------
```

```
      DO 600 J=1,K
      W(J) = 0
      IF(YES.GT.0) THEN
      U(J) = TMIN+J-1
      T(J)=(G/(LOG(((A/U(J))+1)/C)))
      GO TO 4
      ENDIF
      T(J) = TMIN+J-1
4     LAM = LAM1
C*************************************************
      DO 601  I=1,DIV
      V1 = (C1/(LAM*LAM*LAM*LAM*LAM))
      V2 = (C2/(LAM*T(J)))
      V3 = 1/(EXP(V2)-1)
      V4 = (V1*V3)*ARA
      LAM = LAM+ARA
      IF(I.EQ.DIV) THEN
      V4 = (V4/2)
      ENDIF
      W(J) = V4+W(J)
601   CONTINUE
600   CONTINUE
C*************************************************
110   DO 700 J=1,K
      Q(J) = 0
      IF(YES.GT.0) THEN
```

```
      U(J) = TMIN+J-1
      T(J)=(G/(LOG(((A/U(J))+1)/C)))
      GO TO 5
      ENDIF
      T(J) = TMIN+J-1
5     LAM = LAM1
C*************************************************
      DO 701  I=1,DIV
      V1 = (C3/(LAM*LAM*LAM*LAM))
      V2 = (C2/(LAM*T(J)))
      V3 = 1/(EXP(V2)-1)
      V4 = (V1*V3)*ARA
      LAM = LAM+ARA
      IF(I.EQ.DIV) THEN
      V4 = (V4/2)
      ENDIF
      Q(J) = V4+Q(J)
701   CONTINUE
700   CONTINUE
111   J=1
      K=K+1
300   IF(J.LT.K) THEN
      WRITE(1,103) U(J),T(J),Q(J),W(J)
      WRITE(*,103) U(J),T(J),Q(J),W(J)
      J=J+1
103   FORMAT(3X,1F4.1,1X,1F10.3,1X,1G12.4,1X,1F15.8)
```

```
      GO TO 300
      ENDIF
      PRINT *, 'DO YOU WANT TO RUN THE PROGRAM AGAIN'
      PRINT *, 'ENTER 1 FOR YES '
      PRINT *, 'ENTER 0 FOR NO '
      READ *, BIL
      IF(BIL.LT.1) GOTO 998
      GO TO 997
998   STOP
      END
```

APPENDIX B

LISTING OF THE SB2 FORTRAN PROGRAM

```
C     *******PURPOSE*******
C     THIS PROGRAM READS THE TIC–8000 IMAGE FILE AND
C     COMPUTES THE VALUE OF EACH PIXEL AS °C, W/cm² or IU.
C     INPUT IS READ FROM THE FILE CALLED INPUT.IMG
C     SPOT VALUES CAN BE READ FROM SCREEN
C     OUTPUT CAN BE WRITTEN IN A FILE CALLED SB2OUT.MAT
C     AS A 40x40 MATRIX.
      INTEGER N,M,I,J,K,S,RET,BAL,DAL,YES,L,IX,BIL
      INTEGER*1 B(20446)
      REAL RAN,D(140,140),LEV,A,G,C,W,O
998   OPEN(UNIT=99,FILE='a:\input.IMG',
     +ACCESS='DIRECT',STATUS='UNKNOWN',FORM='BINARY',
     +RECL=20446)
      OPEN(UNIT=1 , FILE='SB2OUT.MAT' , STATUS='UNKNOWN' )
      PRINT *, ' HOW  DO YOU WANT OUTPUT    '
      PRINT *, ' ENTER 0 FOR ISOTHERM UNITS '
      PRINT *, ' ENTER 1 FOR TEMPERATURE (°C) '
      PRINT *, ' ENTER 2 FOR IRRADIANCE (W/cm²) '
      READ *, BAL
      IF(BAL.EQ.0) THEN
      GO TO 110
```

```
      ENDIF
      PRINT *, ' ENTER 0 FOR SW '
      PRINT *, ' ENTER 1 FOR LW'
      READ *, DAL
      IF(DAL.LT.1) THEN
      A=811203
      G=3117.74
      C=1
      W=4.69
      W=W*(.00001)
      O=1
      GOTO 110
      ENDIF
      A = -3581
      G = 1506.49
      C = -0.436
      W = 3.03
      W=W/(10000)
      O = 3.624
110   WRITE(*,222) W
222   FORMAT(3X,G15.8)
      PRINT *, ' '
      PRINT *, ' '
      PRINT *, '     READING IMAGE FILE '
      READ (99,REC=1) (B(I),I=1,20446)
102   FORMAT(19600A1)
```

```
      PRINT *,' ENTER RANGE'
      READ *, RAN
      PRINT *,' ENTER LEVEL'
      READ *, LEV
      PRINT *,' '
      PRINT *, 'PLEASE WAIT'
      I=846
      DO 601 J=1,140
      DO 602 K=1,140
      I=I+1
      IF(B(I).LT.0) THEN
      D(J,K)=FLOAT(B(I))
      D(J,K)=256+D(J,K)
      D(J,K)= (((RAN*((D(J,K)-128.5)))/255)+LEV)
      IF(D(J,K).LT.0) THEN
      D(J,K) = 0.000001
      ENDIF
      GO TO 111
      ENDIF
      D(J,K)=FLOAT(B(I))
      D(J,K)= (((RAN*((D(J,K)-128.5)))/255)+LEV)
      IF(D(J,K).LT.0) THEN
      D(J,K) = 0.000001
      ENDIF
111   IF(BAL.EQ.1) THEN
      D(J,K)=(G/(LOG(((A/D(J,K))+1)/C)))
```

```
      D(J,K)=(D(J,K)-273)
      ENDIF
      IF(BAL.EQ.2) THEN
      D(J,K)= W*(D(J,K)+O)
      ENDIF
602   CONTINUE
601   CONTINUE
113   PRINT *, ' DO YOU WANT SPOT VALUE '
      PRINT *, ' ENTER; YES = 1, NO = 0 '
      READ *, YES
      IF(YES.GT.0) THEN
      PRINT *, ' THE COORDINATES OF THE PIXEL'
      PRINT *, ' '
      PRINT *, ' ENTER X, 0≤X≤139 '
      READ *, IX
      PRINT *, ' '
      PRINT *, ' ENTER Y, 0≤Y≤139, (From Down) '
      READ *, M
      S=M
      M=(140-M)
      L=M/2
      L=2*L
      IF(M.GT.L) THEN
      J=((M/2)+71)
      GO TO 114
      ENDIF
```

```
      J=(M/2)
114   K=IX+1
      WRITE(*,115) IX,S,D(J,K)
115   FORMAT(1X,'(',1I3.3,',',1I3.3,') =',F15.8)
      GOTO 113
      ENDIF
      PRINT *,' DO YOU WANT OUTPUT FILE '
      PRINT *,' ENTER; YES = 1, NO = 0 '
      READ *, NO
      IF(NO.LT.1) GOTO 999
117   IF(BAL.GT.0) THEN
109   PRINT *, 'OUTPUT WILL BE WRITTEN IN SB2OUT.MAT'
      PRINT *,' '
      PRINT *,' '
      PRINT *,' '
      PRINT *,' '
      PRINT *,' '
      PRINT *,' '
      DO 118 S=1,100000
118   CONTINUE
      GOTO 116
      ENDIF
      PRINT *, 'OUTPUT WILL BE WRITTEN IN SB2OUT.MAT'
      PRINT *,' '
      PRINT *,' '
      PRINT *,' '
```

```
      PRINT *, ' '
      PRINT *, ' '
      DO 119 S=1,100000
119   CONTINUE
116   M=26
300   IF(M.LT.46) THEN
      J=M+70
      WRITE(1,103) (D(J,K),K=51,90)
      WRITE(*,103) (D(J,K),K=51,90)
      J=M
      WRITE(1,103) (D(J,K),K=51,90)
      WRITE(*,103) (D(J,K),K=51,90)
      M=M+1
103   FORMAT(140F15.8)
      GO TO 300
      ENDIF
999   CLOSE(1)
      PRINT *, ' DO YOU WANT TO RERUN THE PROGRAM '
      PRINT *, ' ENTER; YES = 1, NO = 0 '
      READ *, YES
      IF(YES.LT.1) GOTO 997
      CLOSE(99)
      CLOSE(1)
      GOTO 998
997   STOP
      END
```

APPENDIX C

IMAGE TRANSFER PROCEDURE

A. GENERAL

The thermal image data recorded and stored on the diskettes using the if800 computer were transferred to the IBM–AT Computer using the DISPORT program via a RS–232 interface cable (DISPORT is a registered trademark of GESOTEC Soft– and Hardware GmbH, FRG). The transmission was carried out through the serial ports of the computers using ASCII format. PROCOMM PLUS software program was used to send required commands to the if800 computer (PROCOMM PLUS is a registered trademark of DATASTORM TECHNOLOGIES, INC.). However, any communication program can be used for this purpose.

Data transfer is carried out in blocks. There are two types of blocks. The first type is a block of 252 ASCII characters for the image directory. The organization of the image directory is shown in Table 13. The second type is the thermal image information. The 128 columns by 64 rows of the thermal image are transferred sequentially as bytes starting at the upper left–hand corner of the image. The thermal information of a image is broken down into 64 blocks. Each block has 384 ASCII characters. A code containing three ASCII characters represents the value of one byte. The most significant digit is transferred first and the least significant digit is sent last. Thus, each block contains 128 bytes which represent one row of the thermal image. [Ref. 12]

For a complete description see the Disport Operating Manual [Ref. 12].

TABLE 13. ORGANIZATION OF THE IMAGE DIRECTORY
(Reproduced from Ref. 7)

Param.	Char.No.	stored as	comment
disk label	1,2	Ascii	
im.no.	3-8	16 bit int	image number
RANGE	9-14	16 bit int	
LEVEL	15-20	16 bit int	
abs(A)	21-29	24 bit int	abs(A)=65536*DI(5)+256*DI(6)+DI(7)
B	30-35	16 bit int	
abs(C* 1000)	36-44	24 bit int	abs(C)=(65536*DI(9)+256*DI(10)+ +DI(11))/1000
Dcal*10	45-50	16 bit int	calibration distance (m) dcal=DI(9)/10
sign (A,C)	51-56	16 bit int	bit 0: sign of C bit 1: sign of A
EPS*100	57-62	16 bit int	emissivity obj. * 100
DIS	63-68	16 bit int	object distance (m)
Tamb*10	69-74	16 bit int	ambient temperature (K) * 10
Tatm*10	75-80	16 bit int	atmospheric temperature (K) * 10
TRMS*100	81-86	16 bit int	transmission * 100
alpha* 100000	87-95	24 bit int	alpha=(65536*DI(19)+256*DI(20)+ +DI(21))/100000
beta* 100000	96-104	24 bit int	beta=(65536*DI(22)+256*DI(23)+ +DI(24))/100000
D/R sw	105-110	16 bit int	direct/relative switch 1:relative,0:direct
EPSR*100	111-116	16 bit int	emissivity ref., epsr=DI(14)/100
XR	117-122	16 bit int	horizontal position ref.
YR	123-128	16 bit int	vertical position ref.
VALR	129-134	16 bit int	digital value of reference point
Tref*10	135-140	16 bit int	reference temperature (K) * 10
SCTY	141-146	16 bit int	scanner type
SCVER	147-149	ascii	scanner version
SERNO	150-155	16 bit int	serial no.
FILCOD	156-158	ascii	filter code
FOV*2	159-164	16 bit int	fov=DI(39)/2
APERT*10	165-170	16 bit int	aperture, ap=DI(40)/10
RNO*10	171-176	16 bit int	revision no., rno=DI(41)/10
FI/FRSW	177-182	16 bit int	FIELD/FRAME switch (1=Field, 2=Frame)
image label	183-252	ascii	

B. TRANSFER PROCEDURE

The following is a step–by–step description of the transfer procedure. Figure 26 shows the transfer order of a image data.

* Connect the serial ports of the computers with a RS232 interface cable. There is no need to switch lines in this cable. A straight pin–to–pin connection is all that necessary.

  Turn on both computers.

* Configure the serial port of the if800 computer by using the CONFIG. The standard configuration is
  Baud Rate: 9600, Data Bits: 8, Stop Bits: 1, Parity: NO.

* Load the communication program to the IBM–AT computer and configure the serial port as described in the previous step.

* According to the user manual of the communication program, open a file to write the received ASCII characters.

* Load DISPORT program to the if800 computer. After a short user dialogue, if800 is ready to send.

* In the IBM–AT, be sure you are on the communication screen and everything written onto the screen will be sent to the if800 and will be the content of the file opened. From now on, do not to make any mistake because each key stroke will be written into the file as an ASCII character and will mix with the received image data ASCII characters.

* Send an STX command to the if800 computer from IBM–AT computer. This can be done by typing either ctrl B or Alt 002 (from numeric keyboard).

* If800 responds and begins sending the image directory (252 ASCII characters). See Table 13. At the end of this block the if800 sends an ETX command (ASCII value: 003).

* Send the second STX command. If800 begins to send the thermal image information (384 ASCII characters per block). At the end of each block the if800 sends an ETX command and waits for the next STX command.

* Send an STX command after each ETX command. This procedure continues until 64 blocks of the thermal image have been transferred.

* At the end of the image transfer, DISPORT terminates and ask for another data transfer.

* In the IBM–AT close and save the file. If you want to transfer another image data, open a new file and repeat the transfer steps.

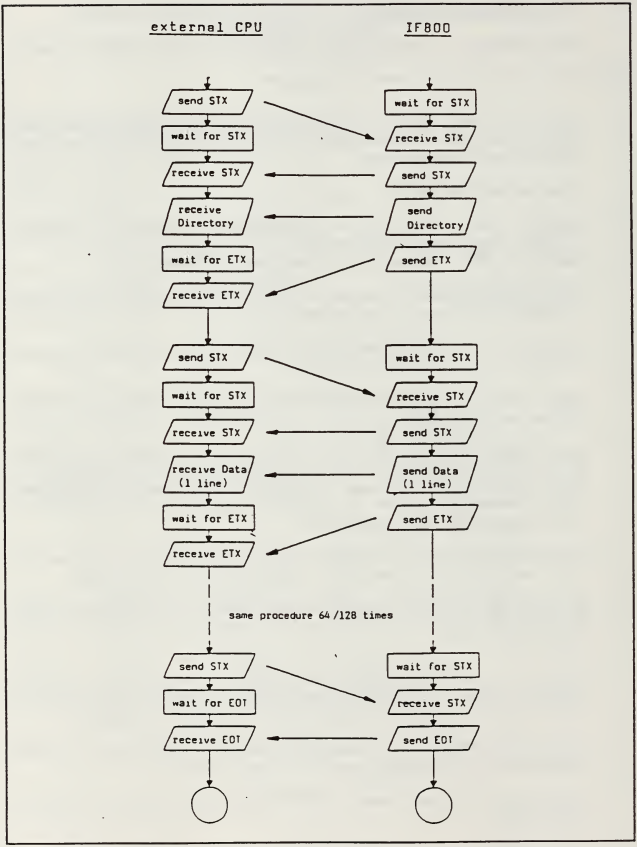

Figure 26. Transfer Order of a Image Data (Reproduced from Ref. 7)

LIST OF REFERENCES

1. Itakura Y., Suteo Tsutsumi and Tohru Takagi, "Statistical Properties of the Background Noise for the Atmospheric Windows in the Intermediate Infrared Region", *Infrared Physics*, v. 14, pp. 17–29, 1974.

2. Manolopoulos, A., *Infrared Background and Target Measurement*, Master's Thesis, Naval Postgraduate School, Monterey, California, December 1985.

3. P. Psihogios, A., *Thermal Images of Sky and Sea–surface Background Infrared Radiation*, Master's Thesis, Naval Postgraduate School, Monterey, California, December 1988.

4. Lloyd, J. M., *Thermal Imaging Systems*, Plenum Press, NY 1975.

5. Ravich, L. E., "Thermal Imaging A Review", *Laser Focus/Electro–optics*, v. 2, pp 98–100, 1 February 1986.

6. Hudson, R. D., Jr., *Infrared System Engineering*, pp. 33–47, John Wiley and Sons, Inc., 1969.

7. Devore, J. L., *Probability and Statistics for Engineering and the Sciences*, pp. 565–575, Brooks/Cole Publishing Company, 1987.

8. *The AGA Thermovision 780 Operating Manual*, Aga Co.

9. Due, Christopher T., *Optical–Mechanical, Active/Passive Imaging Systems – volume II*, ERIM and Office of Naval Research – Department of the Navy, T53200–2–t II, 1982.

10. AGEMA Infrared Systems, *Thermal Image Computer TIC–8000 Operating Manual*, Aga Co.

11. Statistical Graphics Corporation, *Statgraphics User's Guide*, 1988.

12. AGEMA Infrared Systems, *DISCO 3.0 Operating Manual*, Pharos Company, NY, 1989.

INITIAL DISTRIBUTION LIST

		No. Copies
1.	Defense Technical Information Center Cameron Station Alexandria, VA 22304–6145	2
2.	Library, Code 0142 Naval Postgraduate School Monterey, CA 93943–5002	2
3.	Deniz Kuvvetleri Komutanlığı Personel Daire Başkanlığı Bakanlıklar–Ankara / TURKEY	1
4.	Deniz Harp Okulu Komutanlığı Kütüphanesi Tuzla – İstanbul / TURKEY	2
5.	Hava Harp Okulu Komutanlığı Kütüphanesi Yeşilyurt – İstanbul / TURKEY	1
6.	Kara Harp Okulu Komutanlığı Kütüphanesi Bakanlıklar – Ankara / TURKEY	1
7.	Ortadoğu Teknik Üniversitesi Okul Kütüphanesi Ankara / TURKEY	1
8.	Boğaziçi Üniversitesi Okul Kütüphanesi Bebek – İstanbul / TURKEY	1
9.	İstanbul Teknik Üniversitesi Okul Kütüphanesi Ayazağa – İstanbul / TURKEY	1
10.	Professor D. Cleary, Code 61Cl Department of Physics Naval Postgraduate School Monterey, CA 93943	2

11.	Professor A. W. Cooper, Code 61 Cr Department of Physics Naval Postgraduate School Monterey, CA 93943	2
12.	Commander, Naval Sea Systems Command ATTN: PMS 421 CAPT J. Paine Washington, DC 20362–5101	1
13.	U.S. Coast Guard R&D Center ATTN: Frank S. Replogle, Jr. Avery Point, Groton, CT 06340	1
14.	Commander, Naval Environmental Prediction Research Facility ATTN: J. Cook Naval Warfare Support Department Monterey, CA 93943–5006	1
15.	Commander, Naval Environmental Prediction Research Facility ATTN: M. Sierchio Naval Warfare Support Department Monterey, CA 93943–5006	1
16.	Director, Research Administration, Code 012 Naval Postgraduate School Monterey, CA 93943	1
17.	Commanding Officer ATTN: Dr. W. Tolles, Assoc. Dir. of Research Code 1003 Washington, DC 20375–5000	1
18.	Superintendent ATTN: Professor J. Sternberg, Code 73 Naval Postgraduate School Monterey, CA 93943–5000	1
19.	Commander Naval Space and Naval Warfare Systems Command PMW – 145 Washington, DC 20363	1
20.	Yıldızlar Eğt. Mer. Komutanlığı Dz. Tak. Ok. Bşk. Gölcük – Kocaeli /TURKEY	1
21.	Hucumbot Filosu Komutanlığı Birlik Kütüphanesi Umuryeri Beykoz – Istanbul /TURKEY	1

22. Issam Almetlaq 1
P. O. Box 345
Sult/JORDAN

23. Sverker Johnsson 1
c/o Torby
Spanngatan 14
S–58266 Linkoping/SWEDEN

24. Şefik Bayar 2
Feneryolu Mah. Gedikli Sok.
Manolya Apt. No: 7/6
Kızıltoprak – İstanbul /TURKEY